



HAL
open science

Ge coordination in NaAlGe₃O₈ glass upon compression to 131 GPa

Marija Krstulović, Angelika Rosa, Nicole Biedermann, Georg Spiekermann,
Tetsuo Irifune, Manuel Muñoz, Max Wilke

► **To cite this version:**

Marija Krstulović, Angelika Rosa, Nicole Biedermann, Georg Spiekermann, Tetsuo Irifune, et al.. Ge coordination in NaAlGe₃O₈ glass upon compression to 131 GPa. *Physical Review B*, 2020, 101 (21), 10.1103/PhysRevB.101.214103. hal-02951849

HAL Id: hal-02951849



<https://hal.umontpellier.fr/hal-02951849>

Submitted on 29 Sep 2020

HAL is a multi-disciplinary open access archive for the deposit and dissemination of scientific research documents, whether they are published or not. The documents may come from teaching and research institutions in France or abroad, or from public or private research centers.

L'archive ouverte pluridisciplinaire **HAL**, est destinée au dépôt et à la diffusion de documents scientifiques de niveau recherche, publiés ou non, émanant des établissements d'enseignement et de recherche français ou étrangers, des laboratoires publics ou privés.

Ge coordination in NaAlGe₃O₈ glass upon compression to 131 GPa

Marija Krstulović ^{1,2,*}, Angelika D. Rosa,¹ Nicole Biedermann,^{2,3} Georg Spiekermann,² Tetsuo Irifune,⁴ Manuel Muñoz ⁵ and Max Wilke²

¹European Synchrotron Radiation Facility, ESRF, 71 Avenue des Martyrs, 38000 Grenoble, France

²Institute of Geosciences, University of Potsdam, Karl-Liebknecht-Strasse 24–25, 14476 Potsdam-Golm, Germany

³European XFEL, Holzkoppel 4, 22869 Schenefeld, Germany

⁴Geodynamics Research Center, Ehime University Johoku Campus, 2–5 Bunkyocho, Matsuyama, Ehime 790–0826, Japan

⁵Géosciences Montpellier, Université de Montpellier, CNRS, Montpellier, France



(Received 20 December 2019; revised manuscript received 12 May 2020; accepted 13 May 2020; published 4 June 2020)

Structural transformations at high pressure in NaAlGe₃O₈ glass were investigated by means of x-ray absorption spectroscopy at the Ge *K* edge in combination with a diamond anvil cell. The obtained results provide a detailed picture of the local structural behavior of Ge in a chemically complex glass under compression. First and second shell bond distances ($R_{\text{Ge-O}}$ and $R_{\text{Ge...Ge}}$) were extracted assuming contributions of two scattering paths (Ge-O and Ge...Ge). We observed a significant extension of the Ge-O distance from 1.73 to 1.82 Å between 3 and ~26 GPa, accompanied by an increase of the fitted number of nearest neighbors from ~4 to ~6. These observations can be attributed to the change from tetrahedral to octahedral Ge coordination. Second shell bond distances Ge...Ge are also consistent with this structural transformation. Between 34 and 131 GPa, the evolution of the fitted Ge-O distance implies a gradual volume reduction of the Ge octahedra. At the highest probed pressure of 131 GPa a Ge-O distance of 1.73 Å was found, which is similar to the one obtained at ambient conditions for Ge in fourfold coordination. The compressibility of the Ge-O octahedron in NaAlGe₃O₈ beyond 34 GPa is considerably higher than the one reported for amorphous GeO₂ from x-ray diffraction analysis but it is similar to the one reported for the Ge octahedron in crystalline rutile-type GeO₂. We attribute the high compressibility of the Ge-O bond in NaAlGe₃O₈ glass to the presence of Al and Na that increase the system's complexity and therefore its degrees of freedom. Beyond 110 GPa the data on NaAlGe₃O₈ glass indicate the onset of polyhedral distortion. The performed study provides insights into the structural changes of complex and polymerized germanate glasses or melts at extreme pressure conditions.

DOI: [10.1103/PhysRevB.101.214103](https://doi.org/10.1103/PhysRevB.101.214103)

I. INTRODUCTION

Structural properties of germanate glasses under compression have fundamental relevance for our understanding of the compaction mechanism in the polymerized amorphous systems. The questions about the nature of the amorphous-amorphous transitions in germanates is of significant importance in the glass theory, condensed matter physics and chemistry. Germanates are of particular interest in Earth sciences as germanates are considered to be chemical and structural analog materials for silicates, the most abundant mineral group of the Earth's mantle and crust. Their structural proximity to silicate melts makes them suitable analogs for the study of natural melts, including studies at extreme pressure conditions.

Multicomponent silicate melts, and in analogy also germanate melts, are challenging to understand due to complex reciprocal influences of their constituents on the overall physical and chemical melt properties. An important descriptor of this family of melts, that links the structural to the physical properties, is the degree of polymerization of Si-O₄,

Al-O₄ and Ge-O₄ tetrahedra, the main structural units. The degree of polymerization is related to the ratio between oxygen atoms that are bonded to at least two Si/Ge/Al atoms (bridging oxygens, BOs) and those that are bonded to only one Si/Ge/Al atom (nonbridging oxygen atoms, NBOs). From the perspective of the Si/Ge/Al-polyhedron the degree of polymerization is linked to the number of NBOs that these units contain [1]. At low and moderate pressures, the degree of polymerization of tetrahedral units is commonly described as Q^n species, where n corresponds to the number of BOs with n consequently varying between 0 and 4 [1,2]. In pure SiO₂ glass/melt all oxygen atoms are BOs, thus all Si tetrahedra are Q^4 species. In more complex silicate or aluminosilicate glasses that contain also alkali or alkaline earth cations, the dominant Q^n species depends on the abundance of the specific alkali or alkaline earth component and usually a variety of Q^n species is present. While each alkali or alkaline earth component will influence the physical properties of the system in a different way, generally the higher their content, the larger the abundance of smaller n values [1]. As these cations break connections between Si/Ge/Al-tetrahedra, they may have significant influence on the compressional behavior of multicomponent melts and glasses and thus on their physical and chemical properties at high pressure. The influence of

*Corresponding author: krstulov@uni-potsdam.de

depolymerizing components on the compaction mechanism of polymerized and partially depolymerized silicate glasses and melts particularly for pressures up to 5 GPa has been summarized and elucidated in detail in the work by Wolf and McMillan [1]. Many of these studies were performed on melts quenched from high pressure and temperature with subsequent measurements on the glass by various techniques. Important insights were derived from vibrational spectroscopy and magic-angle spinning nuclear magnetic resonance (see Wolf and McMillan [1] and Stebbins [2]). *In situ* investigations at higher pressures were still relatively scarce at that time because of the experimental difficulties, but insights especially by vibrational spectroscopy, were already reported. The study by Williams and Jeanloz [3] reports on structural changes in amorphous SiO₂, CaMgSi₂O₆, and CaAl₂Si₂O₈ up to 31 GPa. It has been shown that structural changes in CaAl₂Si₂O₈ begin at lower pressure compared to SiO₂ and CaMgSi₂O₆, which was related to the presence of Al in CaAl₂Si₂O₈. One year later in a pioneering work, Itie *et al.* [4] studied the coordination change of Ge in GeO₂ up to 20 GPa using x-ray absorption fine-structure (XAFS) technique. Following this study most of previous experimental studies performed at pressures above 7 GPa have been focused on pure oxide compositions GeO₂ [5–7] and SiO₂ [8,9]. These studies provided precise information on the compression behavior of (Ge/Si)O₄ tetrahedra that build the polymeric network at ambient conditions by corner-sharing. Under compression the coordination of Si and Ge changes from tetrahedral to octahedral, and the linkage of these polyhedra changes from corner- to edge-sharing. This transformation is accompanied by the change of oxygen from two- to threefold while still keeping the ideal ratio between the Ge nonbonded radius to the Si/Ge-O bond length [10]. In the picture of the theory of O’Keefe and Hyde on nonbonded forces in crystalline and noncrystalline matter, this is the main driving force for the change in local structure and not the closer packing of oxygens. The repulsive Ge...Ge or Si...Si interactions are also responsible for relatively loosely packed structures of silicates and germanates at ambient conditions.

Despite the fact that amorphous GeO₂ and SiO₂ have been the most studied systems, uncertainties persist on the character of the transition from four- to sixfold (smooth or abrupt) [11,12], the possible existence of a fivefold intermediate coordination state [1,6,11,13,14] and the completion pressure of the four- to sixfold transition [7,15–17]. In some recent studies on GeO₂ and SiO₂ glasses, covering pressures beyond 90 GPa, the appearance of a coordination number higher than six was discussed [9,15,18,19]. The discrepancies between previous studies can be attributed principally to different experimental probe techniques, including x-ray absorption spectroscopy (XAS) and x-ray diffraction (XRD), Brillouin scattering spectroscopy and near-edge spectroscopy by x-ray Raman scattering (XRS). These techniques exhibit a different sensitivity ranging from local changes (XAS, XRS) to bulk observations (XRD, Brillouin). Other sources that could lead to the present disagreements might be the apparent differences in the experimental setups (beamline properties, sample environment) as well as sample synthesis methods.

Only few studies investigated the structural changes in chemically more complex glasses and melts to higher pres-

ures. Among them, Sanloup *et al.* [20] reported on the Si coordination change in molten basalt up to 60 GPa and ~3200 K. This work revealed that the coordination change in basalt is shifted to lower pressures at high temperature compared to glassy SiO₂ which might be explained by the higher chemical complexity and/or temperature [8,21].

In this work, we investigated in detail the structural response of NaAlGe₃O₈ glass up to 131 GPa at room temperature. This glass represents a nominally fully polymerized structure (as GeO₂) due to the coupled substitution of Na and Al for one Ge per formula unit. The coupled substitution of Ge by Na and Al is a first step to increase the complexity of the system while still preserving the polymerization of the tetrahedral network. Notably, the coupled substitution leads to a higher variation of the oxygen-cation bond length and cation-oxygen-cation angles compared to the pure oxides [1]. In our view, this is an ideal way to improve our understanding of compositional effects on the compressional behavior of glasses up to extreme pressures in a systematic way. We performed XAS measurements in this material to determine the atomic environment of Ge, i.e., coordination number and interatomic distances. The composition is in analogy to the naturally occurring tectosilicate mineral albite, NaAlSi₃O₈. Replacing Si by Ge allows for probing the local structure by XAS using a diamond anvil cell (DAC). Low x-ray energies that need to be applied to study light elements like, e.g., Si, Al, Na, Mg, or K are not compatible with high pressure cells. Another advantage of germanate glasses is the fact that structural transitions are shifted to lower pressures compared to silicates [1,4], making the high-pressure phases/state more easily accessible. Even though not all observations on germanates can be completely transferred to silicates [1], this study provides valuable insight to this class of compounds at extreme pressures, in general. Using XAS and a DAC equipped with nanopolycrystalline diamonds [22,23] allowed acquiring high-quality extended x-ray absorption fine structure (EXAFS) spectra up to a *k*-range of 13 Å⁻¹. Particularly, changes in the first and second coordination shell, i.e. bond distances ($R_{\text{Ge-O}}$ and $R_{\text{Ge...Ge}}$) could be followed. Our results suggest, that the onset of the four- to sixfold coordination is slightly shifted to lower pressures and the transformation pressure interval is enlarged compared to observations in pure GeO₂ glass. By using the concept of polyhedral bulk modulus by Hazen and Finger [24,25], we show that the octahedrally coordinated Ge in amorphous NaAlGe₃O₈ preferably undergoes compression up to 110 GPa without polyhedral distortion in contrast to amorphous GeO₂.

II. METHODS

A. Sample synthesis

The NaAlGe₃O₈ glass was synthesized at high temperature using as a starting material a mixture of oxide and carbonate powders in appropriate proportions. Powders were first mechanically homogenized by manual mixing and grinding in an agate mortar for about 5–10 min. The mixture was then placed in a Pt crucible with a Pt lid to prevent devolatilization of alkalis and germanium at high temperatures. The mixture was first annealed at 1050 °C for decarbonization and then

heated up to 1600 °C for 15 h to ensure homogenization of the melt. The Pt crucible was then removed from the furnace and it was immediately immersed in water at ambient temperature in order to quench the melt and to avoid crystallization. This procedure leads to high quenching rates of 400 °C/s favoring a homogeneous glass formation [26]. Raman spectra confirmed the glassy nature of the material.

B. High-pressure XAS experiments

XAS measurements were performed at the micro-XAS station of the beamline BM23 at the European Synchrotron Radiation Facility (ESRF, France) [27]. Two experimental runs on two individual sample loadings were performed, one up to 46 GPa (run 1) and one extending over the pressure range from 14 to 131 GPa (run 2). A double crystal monochromator equipped with two Si(111) crystals in fixed exit geometry was employed for monochromatizing the incoming beam. The x-ray beam was focused down to $5 \times 5 \mu\text{m}^2$ using two Pt coated mirrors inclined to 4 mrad in Kirkpatrick-Baez (KB) geometry that served also as harmonic rejection mirrors. Only for the first run, two Rh coated mirrors in fixed exit and total reflection geometry inclined to 3 mrad, were included in the optical path of the x-rays between the monochromator and the KB-system for additional rejection of higher harmonics. The EXAFS spectra were acquired in transmission mode by scanning the incoming energy across the Ge *K* edge. X-ray beam intensity variations before and after the sample were determined by using ionization chambers filled with appropriate gas mixtures. The energy to monochromator angle was calibrated before and during the experiment using a reference Pt foil placed between the second and third ion chamber. For high-pressure generation, membrane driven Le Toullec-type [28] DACs equipped with nanopolycrystalline diamond anvils were employed [22,23], provided by PRIUS, Geodynamics Research Center, Ehime University, Japan.

These diamonds consist of randomly oriented nanometer-sized crystals, inhibiting contributions of intense Bragg diffraction peaks from single crystal diamond anvils, which would appear as glitches in the XAS spectra. The use of these anvils significantly increased the XAS data quality [29]. All DACs were of Boehler-Almax design [30] with culet diameters of 300 μm for the moderate pressure experiment and 150 μm for the experiment above 100 GPa. For both runs, a rhenium gasket with an initial thickness of 200 μm was indented to a thickness of 50 and 25 μm for the run 1 and 2, respectively. In the center of the indented gasket, a laser-drilled hole served as a sample chamber with diameters of 150 and 75 μm for run 1 and 2, respectively. The sample chamber was filled entirely with the synthetic glass. For hydrostatic pressure generation samples are usually loaded in gas pressure transmitting media, such as He or Ne. However, these gas atoms likely infiltrate the glass, fill the cages of the relatively open network structure and therefore modify its structural response to compression [31]. We therefore conducted the experiments without a pressure transmitting medium to avoid structural incorporation of gas atoms. In both experiments a small sphere of ruby crystal was placed close to the gasket rim, serving as pressure standard up to ~ 100 GPa. The ruby pressure scale with the nonhydrostatic calibration [32] was used to calculate

the pressure from the ruby fluorescence line shift. Beyond 100 GPa, pressure determination from the ruby method was not possible due to the reduced signal intensity and the high fluorescence background from the deformed nanopolycrystalline diamonds. Therefore, at pressures above 100 GPa we acquired diffraction images on the Re-gasket rim at the ID27 diffraction beamline of the ESRF. The beam was then focused to $2 \times 2 \mu\text{m}^2$ and monochromatized to a wavelength of 0.3738 Å. A MarCCD 165 detector was employed, placed at a distance of 191 mm from the sample. Diffraction data were acquired in the oscillation mode, exposing the detector for 10 s during an oscillation of $\pm 5^\circ$. The XRD pressure calculation from Re was based on the Vinet equation of state (EOS) established by Anzellini *et al.* [33] using the PVT-CALC software [34]. This pressure determination method usually provides about 1.2% lower pressures than those prevailing in the center of the sample chamber if He is used as pressure transmitting medium. We assumed a larger pressure uncertainty of 7% as we did not use a pressure medium. Using the correction proposed by Anzellini *et al.* [33], comparable pressure from XRD and ruby fluorescence techniques were obtained for pressures ≥ 100 GPa. Along the entire probed pressure range XAS data were collected in the center of the sample.

C. EXAFS analysis

EXAFS spectra were collected up to 16 \AA^{-1} with a dwell time of 2 and 3 s for run 1 and 2, respectively. The collected EXAFS data were analyzed by the software package XAFS [35]. The background below the Ge *K* edge was subtracted from the spectra by fitting a polynomial function to the pre-edge region (from 11 049 to 11 080 eV). The edge position (E_0) was fitted by a combination of an error function and a Gaussian function. The error function was used to determine the edge position and the edge jump for normalization. The normalized spectra were converted from energy into the *k* space $\chi(k)$. The EXAFS signal (post-edge region) was obtained as $\chi(k) = (\mu - \mu_0)/\mu_0$, with μ as the absorption coefficient and μ_0 was fitted using a smoothing spline function with typically eight knots that were found in order to best minimize low frequencies after background subtraction. EXAFS spectra were k^3 weighted for analysis. The final *k* range used for later analysis extended up to 13 \AA^{-1} . The Fourier transform of the EXAFS function $k^3 \chi(k)$ was performed applying a Kaiser-Bessel window and without phase-shift correction. EXAFS data modeling was performed on unfiltered data. For this analysis, backscattering amplitude and phase shift, as well as photoelectron mean free path, were calculated using the FEFF9 code [36]. The analysis was performed using two coordination shells. In the simplest approach, Ge-O (first) and Ge...Ge (second) coordination shells were used. Two other approaches were tested modifying the contributions to the second shell. This was done by introducing additional scattering paths to the second shell by replacing one Ge by either Al or Na, respectively. The pressure-induced evolution obtained from the latter two approaches did not considerably differ from those of the simple fit model considering Ge-O and Ge...Ge and provided no significant results for Na and Al. In the 6–25 GPa pressure range, structural disorder in the second coordination shell was too high to attain significant

results and fitting of the second shell was therefore omitted. An undistorted tetrahedral configuration for the first coordination shell calculated using FEFF9 served as input structural model in the fits for the entire pressure range. In the pressure range beyond 40 GPa an octahedral configuration was tested but did not provide any significant difference for the fitted parameters, indicating that fit results are independent from the input structural model. The contribution of the second coordination shell was fitted using tetrahedral configuration for pressures up to 3 GPa. Above 25 GPa an octahedral configuration provided better fit results. The fit interval in k space was $3\text{--}13 \text{ \AA}^{-1}$. An asymmetric distribution for the Ge-O and Ge...Ge pair correlation were determined in the fits using an approach implemented in the XAFS software package by Winterer (1997) [35] see Pohlenz *et al.* [37] for details. We found that the inclusion of the asymmetry parameter considerably improves the fits in the pressure range between ~ 8 and ~ 90 GPa, while below 8 and beyond 90 GPa it has a negligible influence on the fit quality. Free fit parameters were the mean bond distances $R_{\text{Ge-O}}$ and $R_{\text{Ge...Ge}}$, Debye-Waller factor σ^2 , and the coordination number for Ge in the first shell ($N_{\text{Ge-O}}$). $N_{\text{Ge...Ge}}$ was constrained to be equal to $N_{\text{Ge-O}}$ in order to reduce the number of fitted parameters. After a first fit with a very small asymmetry parameter (i.e., symmetric distribution), this parameter was iteratively increased until the best fit for each spectrum was obtained. The fit quality was estimated from the χ^2 statistics. The nonstructural parameter ΔE_0 , the energy mismatch between theoretical and experimental scales, was treated as a free fit parameter for the Ge-O scattering path. For Ge...Ge it was constrained to be equal to ΔE_0 obtained for Ge-O value. The amplitude reduction factor S_0^2 was initially constrained to one for all fits by fitting the data set at ambient pressure as well as spectra of crystalline GeO_2 in quartz and rutile structure. The EXAFS signals of the second experimental run showed systematically reduced amplitudes compared to those of the first run spectra. This mismatch might be related to a slightly higher contribution of higher harmonics due to the absence of the Rh-coated mirrors in this run. We, therefore, used an amplitude reduction factor of 0.92 to fit the second dataset in order to account for the presence of a higher fraction of higher harmonics. This procedure led to similar N values extracted from fits of both runs.

III. RESULTS

The normalized absorption spectra in the near-edge region (XANES) are plotted in Fig. 1(a) as a function of increasing pressure up to 121 GPa highlighting the shift of the first XANES peak maximum (FXPM) between 11 110 and 11 130 eV [Fig. 1(a)] and the first EXAFS oscillation [Fig. 1(b)] around 11 180–11 190 eV. The FXPM energy position was determined by fitting a Gaussian curve to the energy region around the maximum ($-4, +1.4$ eV). As the pressure increases, the full width half maximum of the first XANES peak increases and its maximum shifts to higher energies. The strongest changes are observed between 3 and ~ 26 GPa (highlighted by red spectra). In Fig. 1(b) two coupled features can be distinguished in the spectra. While the XANES shoulder around 11 127 eV is very prominent below 3 GPa, it flattens as the pressure increases. As the shoulder flattens

the first EXAFS oscillation shifts towards lower energies and its intensity increases. This feature becomes more prominent beyond 26 GPa.

Figure 2 reports the energy of the maximum of the first XANES peak (denoted as FXPM in [Fig. 1(a)]) as a function of pressure. The total energy shift along the measured pressure range is ~ 3 eV. The evolution of FXPM can be divided in four different regions: At low pressures up to 26 GPa the energy position of FXPM increases steeply with pressure. At 26 GPa the slope of the trend flattens considerably until between 60 and 90 GPa it remains almost constant. Above ~ 90 GPa the FXPM increases again with pressure while a significant scatter of the data points is apparent.

The k^3 -weighted EXAFS function $k^3\chi(k)$ and the corresponding Fourier transform is shown in Figs. 3(a) and 3(b). Up to ~ 20 GPa, the maxima of $\chi(k)$ tend to shift to lower k values. This is pronounced at $\sim 7 \text{ \AA}^{-1}$, and around 9 \AA^{-1} . Upon further compression and beyond 80 GPa, in particular the EXAFS oscillations at $\sim 5 \text{ \AA}^{-1}$ has a significant broadening. Maxima and minima of oscillations at ~ 7 and 9 \AA^{-1} shift towards higher k values beyond 20 GPa. This shift is evident between ~ 40 and ~ 90 GPa and at 9 \AA^{-1} as well as at $\sim 11 \text{ \AA}^{-1}$ [Fig. 3(a)]. In the magnitude of the Fourier transform (R space) of the EXAFS spectra [Fig. 3(b)] the main peak at $\sim 1.3 \text{ \AA}$ corresponds to the signal coming from the first coordination shell, with O atoms as nearest neighbors. Upon compression, this peak shifts to higher R values (interatomic distances uncorrected for phase shift) and becomes broader. The signal beyond the first coordination shell is rather weak, but increases in intensity with pressure due to progressively enhanced contributions from the second coordination shell. In Fig. 4 selected spectra with their corresponding fits are shown covering the fitted k range.

For the interpretation of the data we will show and discuss results of the evolution of the mean bond distances $R_{\text{Ge-O}}$, $R_{\text{Ge...Ge}}$, as well as first shell coordination number $N_{\text{Ge-O}}$. The most reliable parameter for the interpretation of the EXAFS data is the Ge-O distance with an overall uncertainty of $\pm 0.005 \text{ \AA}$. N is directly correlated to the amplitude reduction factor S_0^2 which is not precisely known. Furthermore, the bond distance variance σ^2 (values shown in Table I) is also strongly correlated with N . Thus, the overall uncertainty for the N parameter is about ± 0.5 .

The evolution of the first coordination shell bond distance ($R_{\text{Ge-O}}$) with pressure (Fig. 5) shows a very strong increase up to ~ 26 GPa ($\Delta R \sim 0.09 \text{ \AA}$), whereas between 26 and 34 GPa it is virtually constant ($\Delta R \sim 0.005 \text{ \AA}$) given the uncertainties. Beyond 34 GPa the $R_{\text{Ge-O}}$ decreases constantly up to 131 GPa ($\Delta R \sim 0.09 \text{ \AA}$), whereby its pressure dependence reduces beyond 110 GPa. The coordination number $N_{\text{Ge-O}}$ upon compression is shown in Fig. 6. $N_{\text{Ge-O}}$ exhibits first a strong increase from 4.6 to 6.6, from 1 GPa to 26 GPa, respectively. At higher pressures no further significant change is observed, particularly given the uncertainty for this parameter. Fitted values typically vary between 6.0 and 6.5 in that pressure range.

The pressure evolution of the second coordination shell bond distance $R_{\text{Ge...Ge}}$ is shown in Fig. 7. Up to 3 GPa, tetrahedral coordination dominates, and the obtained mean bond distance is 3.2 \AA , which is in agreement with the reported

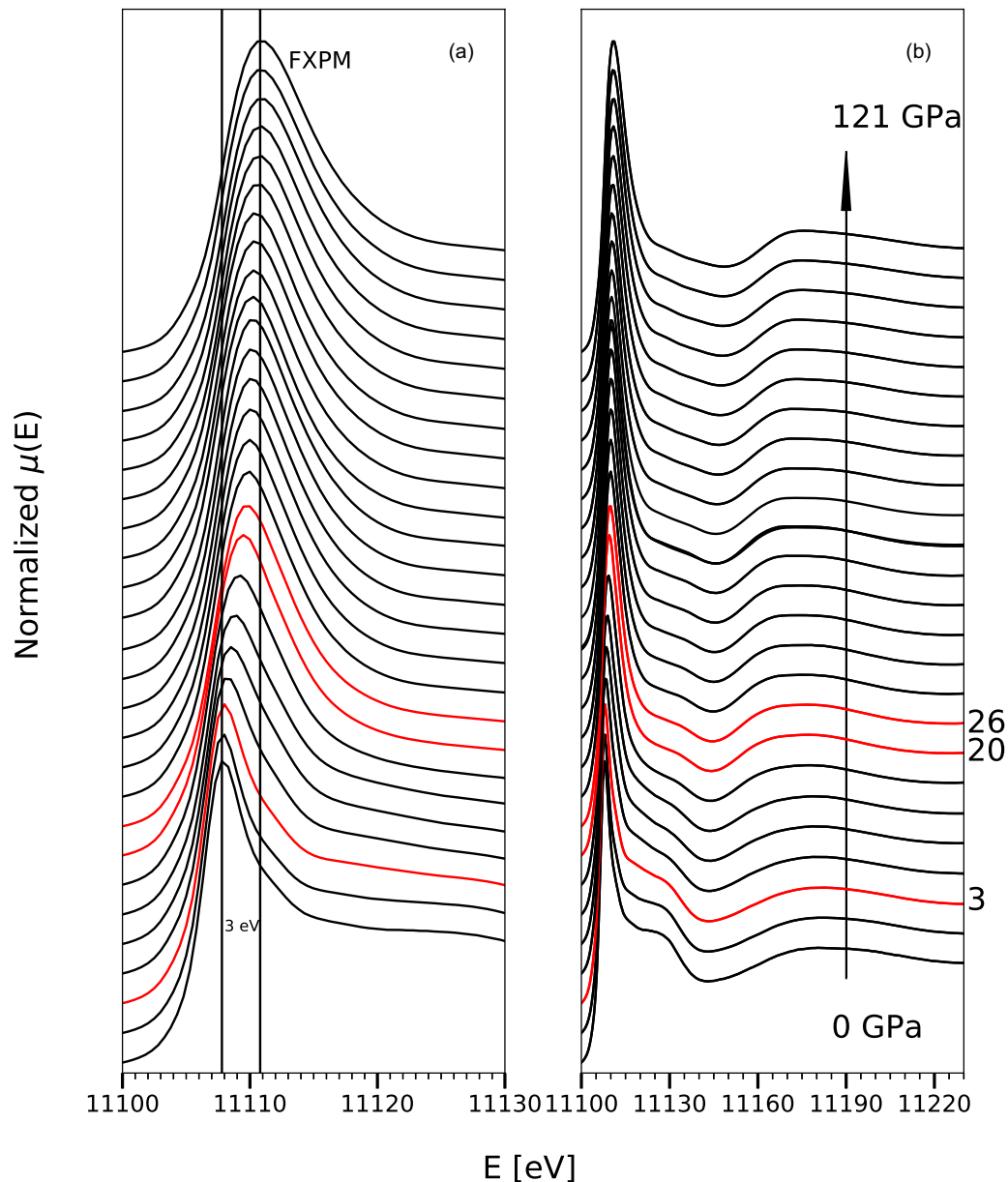


FIG. 1. Normalized Ge K edge XANES spectra as a function of pressure (1–121 GPa). Left side (a) covers the energy range around the first XANES peak maximum (FXPM). The two vertical lines indicate the position of the maximum of the first XANES peak at 0 and 121 GPa, respectively, which exhibits an energy shift of ~ 3 eV over this pressure range. Right side (b) covers the extended energy range between first XANES peak maximum up to 11 240 eV, in which changes in the beginning of the EXAFS region are apparent upon compression. All spectra are shifted along the y axis for clarity. Spectra in red color indicate pressure range with the strongest energy shift (see also Fig. 2).

Ge...Ge bond distance of 3.16 (1) Å in crystalline quartz-type GeO₂ [38]. For the pressure range between 3 and 26 GPa the contribution of the second shell could not be extracted due to the high configurational disorder in the system, this pressure interval is indicated by a grey-shadowed area in Fig. 7. Beyond 26 GPa, distances consistent with edge-sharing Ge octahedra could be fitted for the second shell. The Ge-O pair distribution in our fits can be described as symmetric with low degree of anharmonicity at low pressure (< 8 GPa) with the h parameter 0.01–0.015 as well as at highest pressures ($> \sim 90$ GPa) with an h parameter of 0.02. In the pressure interval between 8 and ~ 90 GPa the pair distribution is asymmetric (for details see Table I).

IV. DISCUSSION

Upon compression, the first neighbor mean Ge-O distance of NaAlGe₃O₈ glass shows a distinctive increase starting at ~ 3 GPa (Fig. 5), which might be due to the onset of the Ge coordination change from tetrahedral to octahedral. The further progressive and significant expansion of the Ge-O distance up to 26 GPa and the increase in the disorder parameter σ^2 (Table I) of the first shell confirm this interpretation and support the assumption of a continuous increase of the Ge coordination number. Fitted results of the second shell mean Ge...Ge distances are in agreement with tetrahedral coordination and polymerization of tetrahedra *via* corners up to 3 GPa [(Fig. 7).

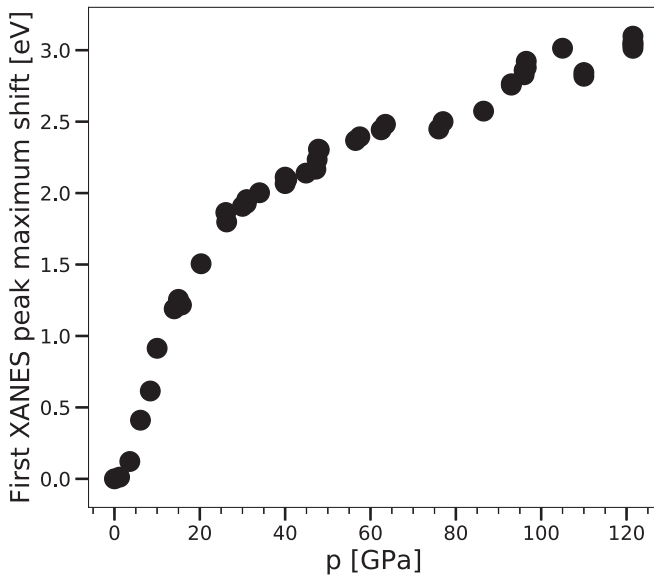


FIG. 2. Energy shift of the fitted first XANES peak maximum (FXPM in Fig. 1) as a function of pressure from 0 to 121 GPa. The point at 131 GPa was not included in this plot due to uncertainties in the energy calibration of the monochromator.

Between 3 and 26 GPa no significant contribution of the second shell can be determined, which may be explained by the high static disorder in the material due to possible coexistence of four-, five-, and sixfold-coordinated Ge in this pressure interval. At higher pressures, the fitted Ge...Ge distances are considerably shorter than below 3 GPa. This is consistent with an arrangement of edge-sharing octahedra like in crystalline rutile [39]. Between 26 and 34 GPa, the mean Ge-O distance exhibits almost no change with pressure. This may indicate that the complete conversion to octahedral coordination of Ge and the structural rearrangement from corner- to edge-sharing polyhedra is reached at 34 GPa. However, the shift of the FXPM with pressure (Fig. 2) indicates a significant change in slope already at 26 GPa and may be taken as evidence that the conversion to octahedral symmetry is already completed around 26 GPa because the XANES region is particularly sensitive to site symmetry. This ambiguity in the data may indicate that the presence of the softer Na-O and Al-O bonds prevents the Ge-O bond length to show a clear turning point in the pressure trend. At pressures beyond 34 GPa, continuous shortening of Ge-O bonds is observed up to 131 GPa with a slight change of the slope beyond 110 GPa.

The mean bond distance presents the most reliable structural parameter extracted from EXAFS. The uncertainty of the fitted N parameter that should describe the number of neighbors has to be considered rather high due to the uncertainty on the nonstructural parameter S_0^2 that also influences the EXAFS amplitude and the correlation of N with the fitted Debye-Waller factor σ^2 . Previous studies showed that the bond length can be used as a sensitive probe for the coordination number as they are correlated *via* the bond-valence theory [37,40–42]. In this theory, the bond valence (s) is directly related to the difference between measured (R) and an empirically determined ideal metal-oxygen bond length (R_0) for a given material according to $s = \frac{R_0 - R}{e^{0.37}}$ [41]. In this sense, the in-

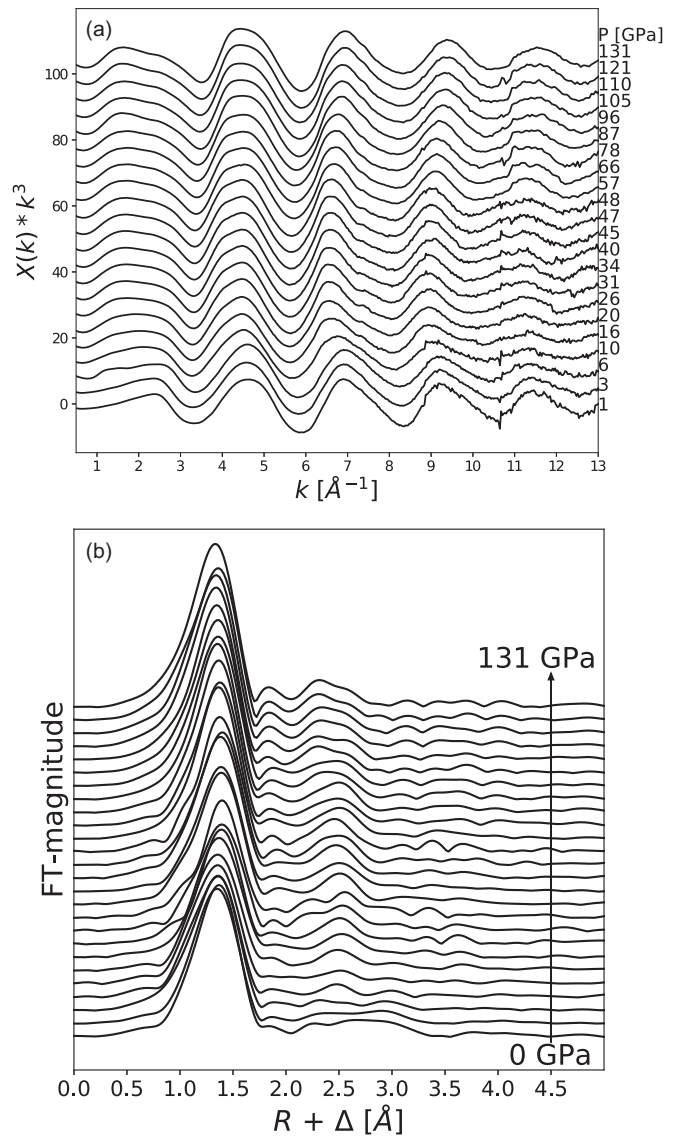


FIG. 3. (a) Evolution of k^3 weighted EXAFS spectra at the Ge K edge of amorphous $\text{NaAlGe}_3\text{O}_8$ upon compression to 131 GPa. (b) Magnitude of the Fourier transform (R) of the EXAFS function shown in (a) of amorphous $\text{NaAlGe}_3\text{O}_8$ to 131 GPa. Plotted data are not corrected for the phase-shift.

crease of the Ge-O distance during conversion to octahedral coordination is dictated by local charge requirements, because compression of the tetrahedral Ge-O units is not possible, as the bond-valence sum around the oxygen atoms would exceed the ideal value of two [10]. Densification at low pressures in these tectosilicate-like structures is accommodated by rearrangement of the polymerized units and rotation of tetrahedra (e.g., Wolf and McMillan, 1995) [1]. Therefore, further compaction is accommodated by rearrangement from loosely packed oxygen atoms in the tectosilicate structure, to a closest packing of oxygen atoms in a rutile-like structure with an edge-sharing configuration of Ge octahedra. During this conversion, the Ge-O expansion is accommodated by the contraction of the nonbonded or next-nearest-neighbor Ge...Ge distance. The strong repulsion of the Ge...Ge interaction is

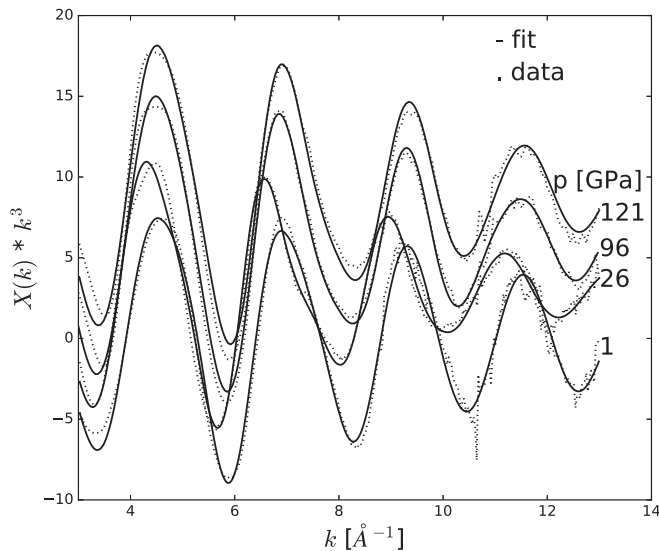


FIG. 4. Selected k^3 weighted EXAFS spectra of amorphous NaAlGe₃O₈ at different pressures and corresponding fits.

overcome by high pressure and is compensated by the increase of the oxygen coordination number from 2 to 3, preserving the ideal value for the oxygen bond valence sum. The structural response of these compounds to pressure can be understood through the relation between the oxygen coordination number and the ratio of the nonbonded Ge radius R_{GeGe} (1.58 Å) [10] and the bonded Ge-O distance $l(R_{\text{GeGe}}/l_{\text{Ge-O}})$, which is developed and described by O'Keefe and Hyde [10]. At room pressure this ratio is ~ 0.91 which meets the requirements for twofold-coordinated oxygen atoms, whereas at 26 GPa and above this ratio is ≤ 0.867 , which satisfies the bond-valence requirements of threefold-coordinated oxygen.

In Fig. 8 we compare the pressure evolution of the average Ge-O distance for amorphous NaAlGe₃O₈ and GeO₂ with the one extracted for rutile-type crystalline GeO₂. Data for GeO₂ glass were determined by Kono *et al.* by XRD [15] and by Hong *et al.* [7] and Baldini *et al.* [16] by EXAFS. Measured data for crystalline GeO₂ in rutile structure up to 25 GPa were taken from Haines *et al.* [39]. We used the concept of polyhedral bulk modulus introduced by Hazen and Finger [24,25] to extrapolate the Ge-O distance of octahedrally coordinated Ge in crystalline rutile-type GeO₂ up to a pressure of 130 GPa. For this calculation, we used a third-order Birch-Murnaghan equation with the parameters $K_{T0} = 270$ GPa and $K'_0 = 7$ [25]. At ambient conditions, NaAlGe₃O₈ and GeO₂ glasses have a similar structure with fully polymerized tetrahedral units connected *via* corners. Due to its higher chemical complexity, the NaAlGe₃O₈ glass has likely a higher structural flexibility than GeO₂ at the same degree of polymerization as only Q^4 species are present in both glasses [1,2]. The data of both glasses, GeO₂ and NaAlGe₃O₈, follow roughly similar trends within the first 40 GPa, showing first a significant expansion, followed by a broad maximum and subsequent decrease of the Ge-O distance. The data coverage from EXAFS does not allow an equivalent evaluation of the influence of Al and Na on the onset of tetrahedral-to-octahedral conversion as reported by Williams and Jeanloz [3] for SiO₂ compared

to CaMgSi₂O₆ and CaAl₂Si₂O₈. Assuming that observations made by Williams and Jeanloz [3] can be transferred to germanates, we suggest that the presence of Al in the structure might favor the shift from four- to sixfold coordination at lower pressure. Further, the high compressibility of the large Na cations could allow for taking up large parts of the structural densification. As a result, the Ge-O (and Al-O) bonds extend, but tetrahedral configuration is preserved. This trend must terminate once the ratio of R_{GeGe}/l reaches the critical threshold and conversion to octahedral coordination starts. These hypotheses could be validated by measurements of the O K edge with x-ray Raman scattering that probes the local structure of oxygen (e.g., Lelong *et al.* [6], Petitgirard *et al.* [21]).

Above 40 GPa, the trend of the Ge-O distance in GeO₂ glass levels off, whereas in NaAlGe₃O₈ it continuously decreases up to the highest pressure with slight change in the slope above 110 GPa. The pressure evolution of the calculated Ge-O distances using the polyhedral bulk modulus can be considered as the one expected for a homogeneously compressed octahedron without any polyhedral distortion. The similarity to the pressure evolution of NaAlGe₃O₈ glass implies that an increase of the Ge coordination number beyond 6 in NaAlGe₃O₈ glass is unlikely as well as distortion of the Ge coordination polyhedron, at least up to ~ 110 GPa. This conclusion is based on the general observation, that an increase of the coordination number should be associated with an increase of the bond length similar to the one observed between 0 and 26 GPa in this study, while polyhedral distortions should result in weaker bond-length reductions with pressure (reduced bond length sensibility with pressure) as illustrated by Spiekermann *et al.* [19] for GeO₂ glass. This simple comparison of the pressure dependence of the Ge-O distance evidences that there is a strong difference in the compressional behavior of the Ge coordination polyhedron between NaAlGe₃O₈ and GeO₂ glass. The weaker shortening of the Ge-O bond distance beyond 110 GPa in NaAlGe₃O₈ might indicate the onset of polyhedral distortions similar to those observed for GeO₂ in the α -PbO₂ structure [43].

In the following, we compare the evolution of the relative bond length with pressure (R_{HP}/R_0) in GeO₂, SiO₂ and NaAlGe₃O₈, which presents the bond length obtained at high pressure normalized to the one at ambient conditions (Fig. 9). This approach reduces systematic errors introduced by using different probe techniques and allows a direct comparison of data on Ge and Si. In NaAlGe₃O₈ glass, this ratio increases during the coordination change to a maximum value of 1.053 where conversion to octahedral coordination is reached. This value is similar to those reported from XAS studies on GeO₂ glass of 1.054 [7] and 1.051 [16]. In the XRD study by Kono *et al.* [15] on GeO₂ glass a larger relative expansion of 1.067 was found. In summary, in the first 26 GPa all compared Ge compounds exhibit a consistent evolution with pressure with the exception of the results obtained by XRD. The origin of these discrepancies may reside in the different sensitivities of the probe techniques. For SiO₂ glass, the relative bond expansion during the four- to sixfold conversion covers a slightly larger pressure interval than in GeO₂ and NaAlGe₃O₈ glass. A considerably higher bond expansion with a factor of 1.08 is obtained by Sato and Funamori [17], whereas the

TABLE I. Values of $R_{\text{Ge-O}}$, $N_{\text{Ge-O}}$, $\sigma_{\text{Ge-O}}^2$, $h_{\text{Ge-O}}$, $R_{\text{Ge...Ge}}$, $N_{\text{Ge...Ge}}$, $\sigma_{\text{Ge...Ge}}^2$, $h_{\text{Ge...Ge}}$ and χ^2 for first and second experimental run at each pressure step. The given pressure up to 100 GPa presents the average of the pressure measured before and after XAS acquisition on the ruby and the uncertainty was calculated from the standard deviation using the nonhydrostatic EOS [32]. For data points above 100 GPa pressure was determined from XRD on the Re gasket before and after XAS acquisitions using the protocol and EOS of Re from Anzellini *et al.*, 2014 [33]. In addition to the standard deviation we assumed a pressure uncertainty of 7% for these points, which is related to the absence of a pressure medium in the present experiments.

Run 1			Run 2		
P [GPa]	$R_{\text{Ge-O}}$ [Å]	$R_{\text{Ge...Ge}}$ [Å]	P [GPa]	$R_{\text{Ge-O}}$ [Å]	$R_{\text{Ge...Ge}}$ [Å]
	$N_{\text{Ge-O}}$	$\sigma_{\text{Ge...Ge}}^2[\text{Å}^2]$		$N_{\text{Ge-O}}$	$\sigma_{\text{Ge...Ge}}^2[\text{Å}^2]$
	$\sigma_{\text{Ge-O}}^2[\text{Å}^2]$	$h_{\text{Ge...Ge}}$		$\sigma_{\text{Ge-O}}^2[\text{Å}^2]$	$h_{\text{Ge...Ge}}$
	$h_{\text{Ge-O}}$			$h_{\text{Ge-O}}$	
	χ^2			χ^2	
1 (0.4)	1.733 (3)	3.2 (4)	14.5 (0.9)	1.796 (3)	2.90 (0.4)
	4.6 (2)	0.021(0)		5.9 (2)	0.0217 (0)
	0.0035 (3)	0.01		0.0044 (4)	0.045
	0.01			0.045	
	0.886			0.544	
3.5 (0.2)	1.735 (2)	3.2 (4)	31.1 (0.4)	1.821 (3)	2.91 (0.4)
	4.8 (1)	0.029 (0)		6.5 (2)	0.0157 (0)
	0.0047 (3)	0.01		0.0030 (4)	0.06
	0.01			0.052	
	0.659			0.585	
6 (0.1)	1.745 (2)		40 (0.2)	1.809 (3)	2.89 (0.4)
	5.2 (1)			6.5 (2)	0.0151 (0)
	0.0058 (3)			0.0038 (4)	0.06
	0.015			0.045	
	0.602			0.604	
8.2 (0.2)	1.769 (3)		48 (0.7)	1.801 (3)	2.91 (0.4)
	5.2 (2)			6.5 (2)	0.0122 (0)
	0.0050 (3)			0.0037 (4)	0.08
	0.035			0.042	
	0.622			0.624	
10 (0.3)	1.780 (3)		57.3 (0.2)	1.784 (3)	2.83 (0.4)
	5.5 (2)			6.3 (2)	0.0182 (0)
	0.0052 (4)			0.0033 (3)	0.04
	0.04			0.040	
	0.601			0.620	
15.4 (0.3)	1.796 (3)		66.3 (0.3)	1.783 (3)	2.82 (0.4)
	5.7 (2)			6.3 (2)	0.0185 (0)
	0.0055 (4)			0.0032 (3)	0.04
	0.04			0.04 (3)	
	0.639			0.653	
20 (0.5)	1.807 (3)	2.9 (3)	76.7 (0.7)	1.774 (3)	2.81 (0.4)
	5.9 (2)	0.021 (0)		6.3 (3)	0.0180 (0)
	0.0054 (4)	0.04		0.0033 (4)	0.05
	0.04			0.040	
	0.537			0.707	
25.6 (0.3)	1.821 (3)	2.9 (3)	86.5 (0.6)	1.751 (3)	2.80 (0.4)
	6.3 (2)	0.020 (0)		6.4 (2)	0.0180 (0)
	0.0038 (3)	0.04		0.0031 (3)	0.05
	0.05			0.020	
	0.629			0.638	

TABLE I. (Continued.)

Run 1			Run 2		
P [GPa]	$R_{\text{Ge-O}}$ [Å]	$R_{\text{Ge...Ge}}$ [Å]	P [GPa]	$R_{\text{Ge-O}}$ [Å]	$R_{\text{Ge...Ge}}$ [Å]
	$N_{\text{Ge-O}}$	$\sigma_{\text{Ge...Ge}}^2[\text{Å}^2]$		$N_{\text{Ge-O}}$	$\sigma_{\text{Ge...Ge}}^2[\text{Å}^2]$
	$\sigma_{\text{Ge-O}}^2[\text{Å}^2]$	$h_{\text{Ge...Ge}}$		$\sigma_{\text{Ge-O}}^2[\text{Å}^2]$	$h_{\text{Ge...Ge}}$
	$h_{\text{Ge-O}}$			$h_{\text{Ge-O}}$	
	χ^2			χ^2	
30.2 (0.3)	1.823 (3)	2.9 (4)	96.2 (0.8)	1.756 (3)	2.84 (0.4)
	6.5 (2)	0.02 (0)		6.5 (2)	0.0088 (0)
	0.0045 (4)	0.04		0.0029 (3)	0.08
	0.05			0.04	
	0.705			0.698	
34.2 (1.0)	1.825 (3)	2.9 (3)	104.9 (2.7)	1.746 (3)	2.83 (0.4)
	6.6 (2)	0.02 (0)		6.3 (2)	0.0149 (0)
	0.0042 (4)	0.04		0.0040 (3)	0.08
	0.05			0.03	
	0.668			0.670	
39.4 (0.7)	1.810 (4)	2.9 (5)	109.6 (4.4)	1.738 (3)	2.82 (0.4)
	6.6 (3)	0.02 (0)		6.2 (2)	0.0147 (0)
	0.0053 (5)	0.04		0.0047 (4)	0.08
	0.04			0.02	
	0.932			0.700	
45.3 (0.2)	1.807 (3)	2.9 (3)	121.4 (5.9)	1.734 (3)	2.81 (0.5)
	6.4 (2)	0.019 (0)		6.4 (3)	0.0147 (0)
	0.0046 (3)	0.04		0.0047 (4)	0.08
	0.04			0.02	
	0.680			0.835	
45.9 (0.7)	1.803 (3)	2.9 (3)	131 (0.5)	1.729 (3)	2.81 (0.5)
	6.4 (2)	0.02 (0)		6.3 (2)	0.0149 (0)
	0.0047 (3)	0.04		0.0047 (3)	0.08
	0.04			0.02	
	0.712			0.730	

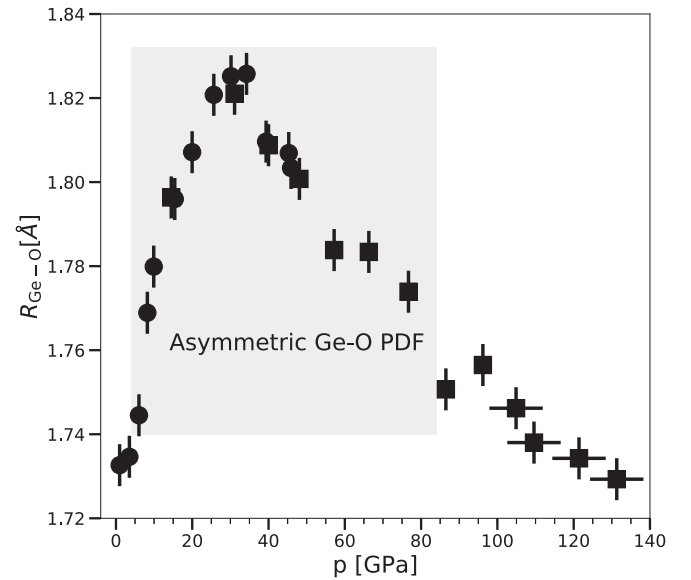


FIG. 5. Evolution of the average Ge-O distance of the first coordination shell ($R_{\text{Ge-O}}$) of amorphous $\text{NaAlGe}_3\text{O}_8$ with pressure, obtained from fitting the experimental spectra acquired in run 1 (circles) and run 2 (squares). The grey shaded area presents the pressure interval in which an asymmetric pair distribution function (PDF) was included in the EXAFS analysis.

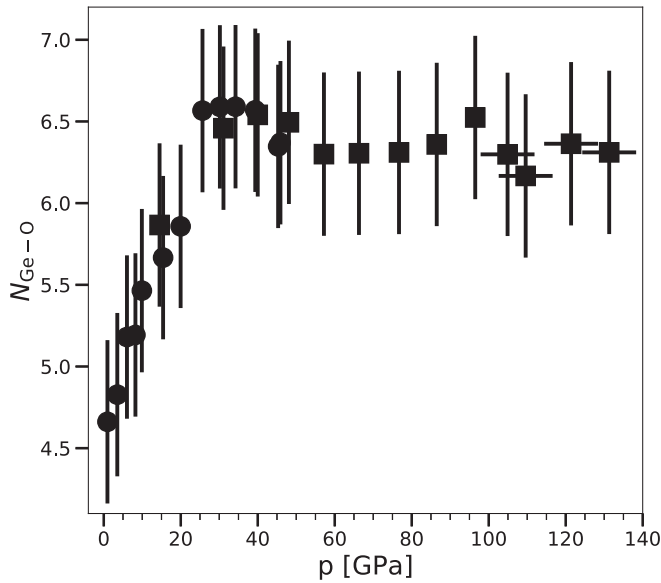


FIG. 6. Evolution of the fitted number of neighbors of the first coordination shell ($N_{\text{Ge-O}}$) of amorphous NaAlGe₃O₈ with pressure. Symbols as in Fig. 5.

factor of 1.059 obtained from the data by Prescher *et al.* [9] is closer to that on GeO₂ glass. The course of the bond distance increase during conversion from four- to sixfold coordination in all compared glass compositions does not necessarily imply the existence of the pure fivefold state. We, however, cannot exclude its presence as a fraction in the mixed-state pressure domain that contains polyhedra with coordination numbers ranging from 4 to 6. The existence of the pure fivefold structure as an intermediate state between four- and sixfold coordination is considered to have significant influence on the

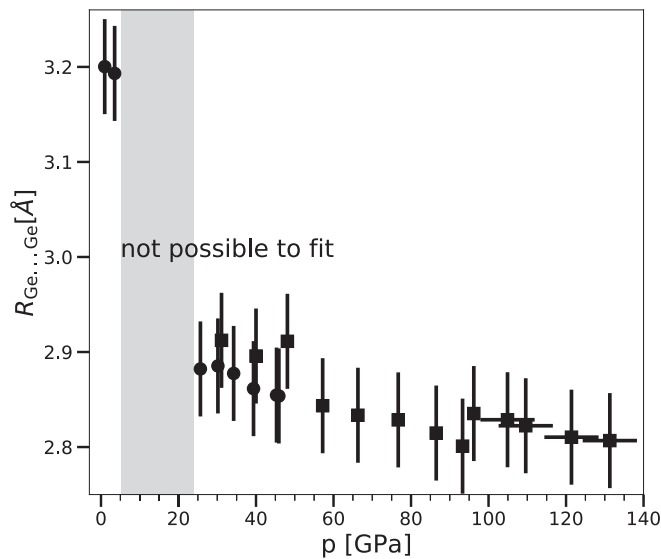


FIG. 7. Evolution of the second coordination shell distance ($R_{\text{Ge}\dots\text{Ge}}$) of amorphous NaAlGe₃O₈ with pressure. Symbols as in Fig. 5. The grey shaded area (between 5.3 and 24 GPa) corresponds to the pressure range in which very high structural disorder in the second coordination shell inhibited the EXAFS analysis.

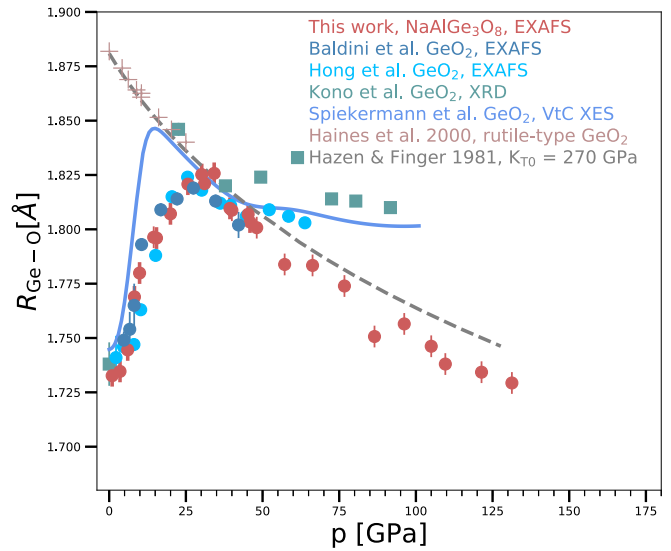


FIG. 8. Evolution of mean Ge-O distances as a function of pressure for amorphous NaAlGe₃O₈ (red symbols) compared to those reported in literature on amorphous GeO₂ (blue symbols) using different probe techniques as indicated (squares for XRD, circles for EXAFS, full line for VtC XES). Data of the mean Ge-O bond length in rutile-type crystalline GeO₂ (sixfold coordinated Ge) are plotted for comparison, including those reported by Haines *et al.* [39] (brown crosses) and those obtained from extrapolation of the compression data reported in Hazen and Finger [25] using a third order Birch-Murnaghan equation of state with $K_{T0} = 270$ GPa and $K'_0 = 7$ [24,25] (grey dashed line).

rheology of a given melt [1]. In previous studies, pure fivefold coordination was reported as an intermediate phase in SiO₂, but not in GeO₂ glass (see chapter by Wolf and McMillan [1]). In some later studies on GeO₂ glasses the presence of fivefold coordination was reported either as a fraction [6], or as a pure intermediate state [11,13]. The present data do not allow deriving a final conclusion on this topic and it is very likely that evidence to constrain the role of fivefold coordination can only be provided by numerical simulations.

Beyond 26 GPa, larger discrepancies are apparent in the Ge/Si-O bond compression evolution: The data of Kono *et al.* [15] as well as those by Spiekermann *et al.* [19] on GeO₂ glass report a smaller bond length reduction with pressure than the one of NaAlGe₃O₈ glass. Data from Hong *et al.* [7] and Baldini *et al.* [16] on GeO₂ glass are similar to the one observed for NaAlGe₃O₈ up to ~40 GPa. Between 40 and 65 GPa the trend for GeO₂ glass levels off. Interestingly, the two data sets on SiO₂ differ in their values at pressures above 26 GPa. The study of Prescher *et al.* [9] exhibits similar pressure evolution as GeO₂ glass [15] along the whole common pressure range, whereas Sato and Funamori [17] reported longer relative bond lengths at given pressures. Compared to NaAlGe₃O₈ glass, the two pure oxide glasses exhibit a lower Ge-O bond-length reduction beyond 40 GPa. As already outlined above, we interpret the trend observed for GeO₂ glass to be due to the fact that compression induces considerable octahedral distortion. Due to the similarity, we may speculate that the Si polyhedron in SiO₂-glass undergoes a similar distortion at extreme pressures as reported for amorphous GeO₂. The

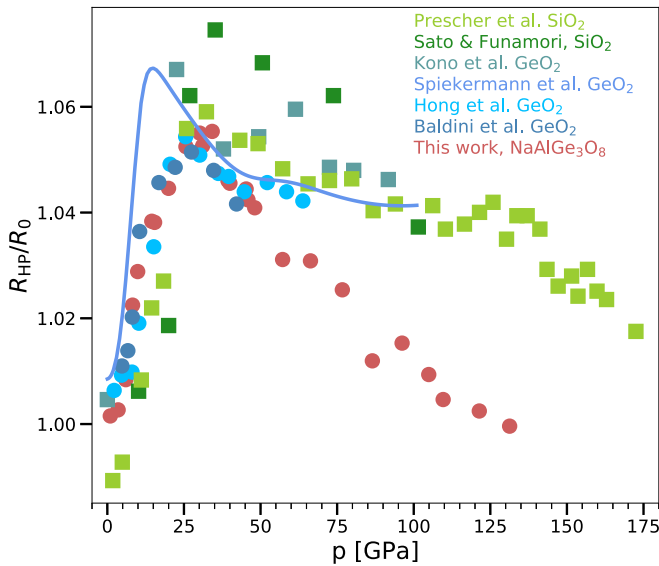


FIG. 9. Evolution of the normalized Ge-O distance expressed by the ratio R_{HP}/R_{P0} of amorphous $\text{NaAlGe}_3\text{O}_8$ with pressure from this study (symbols as in Fig. 8) compared to literature data on the relative changes of the Si-O distance (green symbols) and Ge-O (blue symbols) distances obtained from XRD (squares), EXAFS (circles), and VtC-XES (full line).

very low compressibility in glassy GeO_2 and SiO_2 may be attributed to the presence of only highly charged Ge or Si, which may facilitate octahedral distortion due to stronger intercation repulsion [44]. In contrast to pure oxides, the data on $\text{NaAlGe}_3\text{O}_8$ glass show a trend that may be easily interpreted by mere compression of largely undistorted Ge octahedra. This simpler compressional behavior might be related to the presence of Na and Al. The charge difference between Al and Ge leads to a longer mean bond length for Al-O due to its lower bond strength according to the bond strength theory [41]. Similarly, a significantly larger mean bond length for Na compared to Ge-O can be considered due to its higher coordination number [45]. In contrast to Ge-O, the nonbonded Ge...Ge distance shows only little shortening at pressures beyond the completion of the octahedral coordination (Fig. 7). We do admit that describing the second shell in our EXAFS fits with Ge...Ge only represents a simplification. Still, considering the concepts of O'Keefe and Hyde [10,44,46] we may speculate that after conversion to sixfold coordination at ~ 26 GPa, the critical threshold distance between nonbonded Ge...Ge is reached, between two edge-sharing octahedra. Thus, closer packing and overall volume reduction is now achieved by the reduction of the Ge-O, Ge...Al and Ge...Na bond lengths. As an example, one could consider an oxygen atom that links three octahedra, two edge-sharing octahedra, one Ge and one Al, and an adjacent Ge octahedron. Volume reduction, and therefore average Ge-O bond-length reduction,

can be achieved *via* bond angle adjustments, i.e., increase of Al-O-Ge angle and Al-O distance. This would lead to a decrease of the two Ge-O bond distances accommodating the oxygen bond valence, and to reduction of the nonbonded Al...Ge distance that was not yet at its critical threshold value, in contrast to Ge...Ge.

Earlier studies have already shown that aluminosilicate glasses exhibit a distinct structure evolution to the pure silica system [3], e.g., shifting conversion from tetrahedral to octahedral coordination to lower pressure. Addition of Al and Na to GeO_2 leads to an overall decrease of the average bond valence sum of the oxygen atoms in the structure and thus, to a higher structural flexibility that can explain the observed increased compressibility compared to GeO_2 . The question at which pressure $\text{NaAlGe}_3\text{O}_8$ glass will also show polyhedral distortion for Ge cannot be conclusively answered from our data, but the apparent flattening of the bond distance evolution beyond 110 GPa might indicate the onset of octahedral distortion.

The results on the complex fully polymerized $\text{NaAlGe}_3\text{O}_8$ glass reported here indicate that chemically complex germanate (and in analogy also silicate), glasses will exhibit a structural behavior upon compression that is considerably different from that observed for the pure oxide compositions GeO_2 and SiO_2 . The local structure evolution with pressure found in the simple compound studied here provides insight into the compaction mechanism of fully polymerized alkali aluminogermanate glasses. This includes insight into the four- to sixfold amorphous-amorphous phase transition as well as the densification mechanism that acts far beyond the transition to octahedral coordination. Our observations suggest that glasses or melts with even higher chemical complexity than $\text{NaAlGe}_3\text{O}_8$ may follow similar trends and are very distinct to the pure GeO_2 system.

ACKNOWLEDGMENTS

We thank the anonymous reviewers for their very constructive comments and the editor for fast handling of the manuscript. We are particularly grateful for pointing us to the unique concept of nonbonded forces that seem to have been forgotten in textbooks on crystal chemistry. We thank the entire staff of the beamline BM 23 of the European Synchrotron Radiation Facility (ESRF), in particular S. Pascarelli and O. Mathon, for providing us two experimental sessions to perform the experiment. We strongly recognize the technical support provided by F. Perrin and S. Pasternak. We also thank M. Mezouar and G. Garbarino for their help with XRD measurements at ID27. We warmly thank also J. Jacobs from the high-pressure sample environment for his assistance with high-pressure instrumentation, and R. Torchio for providing the measurements on reference samples. M.W. would like to acknowledge funding by DFG through Project Wi 2000/13-1.

[1] G. H. Wolf and P. F. McMillan, Pressure effects on silicate melt structure and properties, in *Structure, Dynamics and Properties of Silicate Melts*, edited by J. F. Stebbins, P. F. McMillan, and D. B. Dingwell (Mineralogical Society of America, Washington, DC, 1995), Chap. 11, Vol. 32, p. 505.

[2] J. F. Stebbins, Dynamics and structure of silicate and oxide melts: Nuclear magnetic resonance studies, in *Structure, Dynamics and Properties of Silicate Melts*, edited by J. F. Stebbins, P. F. McMillan, and D. B. Dingwell (Mineralogical Society of America, Washington, D.C., 1995), Chap. 7, Vol. 32, p. 191.

- [3] Q. Williams and R. Jeanloz, Spectroscopic evidence for pressure-induced coordination changes in silicate glasses and melts, *Science* **239**, 902 (1988).
- [4] J. P. Itié, A. Polian, G. Calas, J. Petiau, A. Fontaine, and H. Tolentino, Pressure-Induced Coordination Changes in Crystalline and Vitreous GeO₂, *Phys. Rev. Lett.* **63**, 398 (1989).
- [5] F. Vannereau, J. P. Itié, A. Polian, G. Calas, J. Petiau, A. Fontaine, and H. Tolentino, Pressure-Induced coordination changes of germanium in crystalline and vitreous germanates, *High Press. Res.* **7**, 372 (1991).
- [6] G. Lelong, L. Cormier, G. Ferlat, V. Giordano, G. S. Henderson, A. Shukla, and G. Calas, Evidence of fivefold-coordinated Ge atoms in amorphous GeO₂ under pressure using inelastic x-ray scattering, *Phys. Rev. B* **85**, 134202 (2012).
- [7] X. Hong, M. Newville, T. S. Duffy, S. R. Sutton, and M. L. Rivers, X-ray absorption spectroscopy of GeO₂ glass to 64 GPa, *J. Phys. Condens. Matter* **26**, 035104 (2014).
- [8] H. Fukui, M. Kanzaki, N. Hiraoka, and Y. Q. Cai, Coordination environment of silicon in silica glass up to 74 GPa: An x-ray Raman scattering study at the silicon *L* edge, *Phys. Rev. B* **78**, 012203 (2008).
- [9] C. Prescher, V. B. Prakapenka, J. Stefanski, S. Jahn, L. B. Skinner, and Y. Wang, Beyond sixfold coordinated Si in SiO₂ glass at ultrahigh pressures, *Proc. Natl. Acad. Sci.* **114**, 10041 (2017).
- [10] M. O'Keefe and B. G. Hyde, The role of nonbonded forces in crystals, in *Structure and Bonding in Crystals*, edited by M. O'Keefe and A. Navrotsky (Academic Press Inc., New York, 1981), Chap. 10, Vol. 1, p. 227.
- [11] D. Marrocchelli, M. Salanne, and P. A. Madden, High-pressure behavior of GeO₂: A simulation study, *J. Phys. Condens. Matter* **22**, 152102 (2010).
- [12] M. Vaccari, G. Aquilanti, S. Pascarelli, and O. Mathon, A new EXAFS investigation of local structural changes in amorphous and crystalline GeO₂ at high pressure, *J. Phys.: Condens. Matter* **21**, 145403 (2009).
- [13] M. Guthrie, C. A. Tulk, C. J. Benmore, J. Xu, J. L. Yarger, D. D. Klug, J. S. Tse, H.-k. Mao, and R. J. Hemley, Formation and Structure of a Dense Octahedral Glass, *Phys. Rev. Lett.* **93**, 115502 (2004).
- [14] T. Sato, N. Funamori, D. Wakabayashi, K. Nishida, and T. Kikegawa, Coexistence of two states in optically homogeneous silica glass during the transformation in short-range order, *Phys. Rev. B* **98**, 144111 (2018).
- [15] Y. Kono, C. Kenney-Benson, D. Ikuta, Y. Shibazaki, Y. Wang, and G. Shen, Ultrahigh-pressure polyamorphism in GeO₂ glass with coordination number >6, *Proc. Natl. Acad. Sci. USA* **113**, 3436 (2016).
- [16] M. Baldini, G. Aquilanti, H. K. Mao, W. Yang, G. Shen, S. Pascarelli, and W. L. Mao, High-pressure EXAFS study of vitreous GeO₂ up to 44 GPa, *Phys. Rev. B* **81**, 024201 (2010).
- [17] T. Sato and N. Funamori, High-pressure structural transformation of SiO₂ glass up to 100 GPa, *Phys. Rev. B* **82**, 184102 (2010).
- [18] M. Murakami and J. D. Bass, Spectroscopic Evidence for Ultrahigh-Pressure Polymorphism in SiO₂ Glass, *Phys. Rev. Lett.* **104**, 025504 (2010).
- [19] G. Spiekermann, M. Harder, K. Gilmore, P. Zalden, C. J. Sahle, S. Petitgirard, M. Wilke, N. Biedermann, C. Weis, W. Morgenroth, J. S. Tse, E. Kulik, N. Nishiyama, H. Yavas, and C. Sternemann, Persistent Octahedral Coordination in Amorphous GeO₂ up to 100 GPa by K β'' X-ray Emission Spectroscopy, *Phys. Rev. X* **9**, 011025 (2019).
- [20] C. Sanloup, J. W. E. Drewitt, Z. Konôpková, P. Dalladay-Simpson, D. M. Morton, N. Rai, W. van Westrenen, and W. Morgenroth, Structural change in molten basalt at deep mantle conditions, *Nature (London)* **503**, 104 (2013).
- [21] S. Petitgirard, C. J. Sahle, C. Weis, K. Gilmore, G. Spiekermann, J. S. Tse, M. Wilke, C. Cavallari, V. Cerantolla, and C. Sternemann, Magma properties at deep Earth's conditions from electronic structure of silica, *Geochem. Persp. Lett.* **9**, 32 (2019).
- [22] T. Irifune, A. Kurio, S. Sakamoto, T. Inoue, and H. Sumiya, Materials: Ultrahard polycrystalline diamond from graphite, *Nature* **421**, 599 (2003).
- [23] N. Ishimatsu, K. Matsumoto, H. Maruyama, N. Kawamura, M. Mizumaki, H. Sumiya, and T. Irifune, Glitch-free X-ray absorption spectrum under high pressure obtained using nanopolycrystalline diamond anvils, *J. Synchrotron Radiat.* **19**, 768 (2012).
- [24] R. M. Hazen and L. W. Finger, Bulk Modulus-Volume Relationship for Cation-Anion Polyhedra, *J. Geophys. Res.* **84**, 6723 (1979).
- [25] R. M. Hazen and L. W. Finger, Bulk moduli and high-pressure crystal structures of rutile-type compounds, *J. Phys. Chem. Solids* **42**, 143 (1981).
- [26] D. P. Birnie III and M. D. Dyar, Cooling rate calculations for silicate glasses, *J. Geophys. Res., California* **91**, D509 (1986).
- [27] O. Mathon, A. Beteva, J. Borrel, D. Bugnazet, S. Gatla, R. Hino, I. Kantor, T. Mairs, M. Munoz, S. Pasternak, F. Perrin, and S. Pascarelli, Radiation Facility: the general-purpose EXAFS bending-magnet beamline BM23, *J. Synchrotron Radiat.* **22**, 1548 (2015).
- [28] R. Letoullec, J. P. Pinceaux, and P. Loubeyre, The membrane diamond anvil cell: A new device for generating continuous pressure and temperature variations, *High Press. Res.* **1**, 77 (1988).
- [29] A. D. Rosa, O. Mathon, R. Torchio, J. Jacobs, S. Pasternak, T. Irifune, and S. Pascarelli, Nano-polycrystalline diamond anvils: Key devices for XAS at extreme conditions: their use, scientific impact, present status and future needs, *High Press. Res.* **40**, 65 (2019).
- [30] R. Boehler and K. De Hantsetters, New anvil designs in diamond-cells, *High Press. Res.* **24**, 391 (2004).
- [31] G. Shen, Q. Mei, V. B. Prakapenka, P. Lazor, S. Sinogeikin, Y. Meng, and C. Park, Effect of helium on structure and compression behavior of SiO₂ glass, *Proc. Natl. Acad. Sci.* **108**, 6004 (2011).
- [32] H. K. Mao, P. M. Bell, J. W. Shaner, and D. J. Steinberg, Specific volume measurements of Cu, Mo, Pd, and Ag and calibration of the ruby R1 fluorescence pressure gauge from 0.06 to 1Mbar, *J. Appl. Phys.* **49**, 3276 (1978).
- [33] S. Anzellini, A. Dewaele, F. Occelli, P. Loubeyre, and M. Mezouar, Equation of state of rhenium and application for ultrahigh pressure calibration, *J. Appl. Phys.* **115**, 043511 (2014).
- [34] J. Gonzalez-Platas, M. Alvaro, F. Nestola, and R. Angel, EosFit7-GUI: a new graphical user interface for equation of state calculations, analyses and teaching, *J. Appl. Crystallography* **49**, 1377 (2016).

- [35] M. Winterer, XAFS - a data analysis program for materials science in proceedings of the 9th international conference on x-ray absorption fine structure, *J. Phys. IV France* **7**, C2-243 (1997).
- [36] J. J. Rehr, J. J. Kas, F. D. Vila, M. P. Prange, and K. Jorissen, Parameter-free calculations of x-ray spectra with FEFF9, *Phys. Chem. Chem. Phys.* **12**, 5503 (2010).
- [37] J. Pohlenz, A. D. Rosa, O. Mathon, S. Pascarelli, S. Belin, G. Landrot, V. Murzin, A. Veligzhanin, A. Shiryaev, T. Irifune, and M. Wilke, Structural controls of CO₂ on Y, La and Sr incorporation in sodium-rich silicate - carbonate melts by *in-situ* high P-T EXAFS, *Chem. Geology* **486**, 1 (2018).
- [38] M. Micoulaut, L. Cormier, and G. S. Henderson, The structure of amorphous, crystalline and liquid GeO₂, *J. Phys.: Condens. Matter* **18**, R753 (2006).
- [39] J. Haines, J. M. Leger, C. Chateau, and A. S. Pereira, Structural evolution of rutile-type and CaCl₂-type germanium dioxide at high pressure, *Phys. Chem. Miner.* **27**, 575 (2000).
- [40] L. Pauling, The principles determining the structure of complex ionic crystals, *J. Am. Chem. Soc.* **51**, 1010 (1929).
- [41] I. D. Brown, Recent developments in the methods and applications of the bond valence model, *Chem. Rev.* **109**, 6858 (2009).
- [42] S. Simon, M. Wilke, R. Chernikov, S. Klemme, and L. Hennet, The influence of composition on the local structure around yttrium in quenched silicate melts - Insights from EXAFS, *Chem. Geology* **346**, 3 (2013).
- [43] R. Dutta, C. E. White, E. Greenberg, V. B. Prakapenka, and T. S. Duffy, Equation of state of the α -PbO₂ and Pa $\bar{3}$ -type phases of GeO₂ to 120 GPa, *Phys. Rev. B* **98**, 144106 (2018).
- [44] M. O'Keeffe and B. G. Hyde, On Si-O-Si configurations in silicates, *Acta Crystallogr.* **B34**, 27 (1978).
- [45] F. Farges, S. de Wispelaere, S. Rossano, M. Muñoz, M. Wilke, A. M. Flank, and P. Lagarde, Local structures around Si, Al and Na in hydrated silicate glasses, in *X-RAY ABSORPTION FINE STRUCTURE - XAFS13: 13th International Conference*, edited by B. Hedman and P. Pianetta, AIP Conf. Proc. No. 882 (American Institute of Physics, New York, 2007), p. 214.
- [46] B. G. Hyde, Inorganic and mineral structures reconsidered, *J. Proc. Roy. Soc. New South Wales* **119**, 153 (1986).